of **1**; 15 mol of **2**/mol of **1** was used. After the reagents were mixed, spectral changes were observed similar to those seen in the reaction run in pure methanol, the main difference being a faster decay of the quinone methide absorbance. The rate of decay of the absorbance at 648 nm, over a range from 60% to 20% of its maximum intensity, was fitted to the rate law expressed by eq 1, by a nonlinear least-squares fitting procedure. The results are reported in Table II. In each experiment, when the reaction was over, the cell was opened and the solution analyzed by HPLC. 7-Deoxynogarol (**5**) and bi(7-deoxynogarol-7-yl) (**6**) in ca. 3.5/1 ratio accounted for about 90% of the total peak area. Part of **5** and **6** appeared in their leuco[31] forms, especially when the cell had been opened several hours after the disappearance of the quinone methide absorbance.

Reaction of Menogaril (1) with 0.33 Mole Equivalent of DHM-3 Dimer (4) in the Presence of *N*-Acetyl-L-cysteine in Water. DHM-3 dimer (**4**; 0.036 mg, 1.15×10^{-4} mmol) was loaded into the cuvette portion of a two-compartment cell as described in the General Remarks paragraph. The degassing chamber was loaded with 2.5 mL of a solution 1.38×10^{-4} M in **1**, 3.75×10^{-2} M in *N*-acetyl-L-cysteine, 8.0×10^{-2} M in Tris, and 1.4×10^{-3} M in Tris·HCl. The solvent was 5% v/v dimethylformamide in water, and the pH of the solution was 8.2. After freeze–thaw degassing and sealing under vacuum, the cell was brought to 25 °C. The reactants were mixed, the cell was placed in the cell holder of the UV–vis spectrometer thermostated at 25.0 ± 0.1 °C, and spectra were taken periodically. A partial decrease of the quinone band at 472 nm coupled with the appearance of a hydroquinone absorption band at 426 nm was observed. The quinone band reached a minimum (1.3 from the original 1.7 absorbance) after ca. 400 s. After ca. 6000 s the quinone band began to increase very slowly at the expense of the hydroquinone band, which had reached its maximum intensity (absorbance 1.6). After an additional 70 h, the absorption maximum of the quinone had reached a value of 1.4 while the hydroquinone band appeared as a shoulder with an intensity of 1.2 absorption units. During the course of the reaction no absorption band for quinone methide, expected at ca. 600 nm, was observed. After a total of 72 h the cell was opened and the solution was analyzed by HPLC. The chromatogram showed the same two peaks, at 1.5 and 1.9 min, observed for the menogaril–cysteine diastereoisomeric adducts (**10**) found from the reaction of **1**, **2**, and *N*-acetyl-L-cysteine in methanol, as reported previously. These two peaks accounted for 80% of the total area. A minor peak corresponding to **5** was also present accounting for 9% of the total area. No unreacted menogaril (**1**) was detected.

Magnetic Exchange Interactions in Semiquinone Complexes of Iron. Structural and Magnetic Properties of Tris(3,5-di-*tert*-butylsemiquinonato)iron(III) and Tetrakis(3,5-di-*tert*-butylsemiquinonato)tetrakis(3,5-di-*tert*-butylcatecholato)tetrairon(III)

Steven R. Boone,[1] Gordon H. Purser,[1] Hsiu-Rong Chang,[2] Michael D. Lowery,[2] David N. Hendrickson,*[,2] and Cortlandt G. Pierpont*[,1]

Contribution from the Department of Chemistry and Biochemistry, University of Colorado, Boulder, Colorado 80309, and the School of Chemical Sciences, University of Illinois, Urbana, Illinois 61801. *Received May 27, 1988*

Abstract: Iron–semiquinone magnetic interactions have been studied in complexes obtained from the reaction between $Fe(CO)_5$ and 3,5-di-*tert*-butyl-1,2-benzoquinone (DBBQ). The green product formed when DBBQ is used in excess is $Fe(DBSQ)_3$; when $Fe(CO)_5$ is used in excess, blue $Fe_4(DBSQ)_4(DBCat)_4$ is obtained. Mössbauer spectra for both complexes indicate that they contain high-spin Fe(III) ions. The X-ray structure of $Fe(DBSQ)_3$ shows that the molecule has C_3 symmetry with metrical values consistent with the tris(semiquinonate)iron(III) charge distribution. The structure of centrosymmetric $Fe_4(DBSQ)_4(DBCat)_4$ consists of a planar arrangement of iron atoms, resembling two triangles sharing a common edge. Semiquinone and catecholate ligands are clearly distinguishable by their structural features. Oxygen atoms of the ligands bridge edges of the triangles, and one catecholate oxygen is located atop each triangle, bridging three metal ions. The magnetic moment of $Fe(DBSQ)_3$ is 2.9 μ_B consistent with the $S = 1$ ground state that arises from strong coupling between the $S = {}^5/_2$ metal ion and the three $S = {}^1/_2$ ligands. The tetranuclear complex shows temperature-dependent magnetic behavior with an effective moment of 5.94 μ_B per molecule at 321 K which decreases to 0.72 μ_B at 5 K. This arises both from iron–semiquinone coupling and from antiferromagnetic coupling between Fe(DBSQ)(DBCat) monomeric units of the molecule.

Metal complexes containing paramagnetic organic ligands have been confined primarily to nitroxyl ligands[3] and unsaturated imines including porphyrins[4] and bipyridine.[5] Over the past several years we have been able to show that the *o*-semiquinones have a rich coordination chemistry. Complexes consisting of both paramagnetic metal ions and radical semiquinone ligands have been of particular interest in these studies. Reactions carried out between the neutral metal carbonyl complexes $Cr(CO)_6$ and $Fe(CO)_5$ and the *o*-benzoquinones 3,5-di-*tert*-butyl-1,2-benzoquinone, tetrachloro-1,2-benzoquinone, and 9,10-phenanthrenequinone gave neutral tris(quinone) products.[6,7] At the time that these compounds were synthesized, the intramolecular distribution of charge remained unclear even though structural information was available.[8] Subsequent results of characterization using

(1) University of Colorado.
(2) University of Illinois.
(3) (a) Caneschi, A.; Gatteschi, D.; Laugier, J.; Rey, P.; Sessoli, R.; Zanchini, C. *J. Am. Chem. Soc.* **1988**, *110*, 2795. (b) Caneschi, A.; Grand, A.; Langier, J.; Rey, P.; Subra, R. *J. Am. Chem. Soc.* **1988**, *110*, 2307. (c) Porter, L. C.; Dickman, M. H.; Doedens, R. J. *Inorg. Chem.* **1988**, *27*, 1548.
(4) (a) Phillippi, M. A.; Goff, H. M. *J. Am. Chem. Soc.* **1982**, *104*, 6026. (b) Scholz, W. F.; Reed, C. A.; Lee, Y. J.; Scheidt, W. R.; Lang, G. *J. Am. Chem. Soc.* **1982**, *104*, 6791. (c) Buisson, G.; Deronzier, A.; Duee, E.; Gans, P.; Marchon, J.-C.; Regnard, J.-R. *J. Am. Chem. Soc.* **1982**, *104*, 6793.
(5) (a) Gex, J. N.; DeArmond, M. K.; Hanck, K. W. *Inorg. Chem.* **1987**, *26*, 3235. (b) Wulf, V. E.; Herzog, S. *Z. Anorg. Allg. Chem.* **1972**, *387*, 81. (c) Hanzaki, I.; Nagakura, S. *Bull. Chem. Soc. Jpn.* **1971**, *44*, 2312.
(6) Pierpont, C. G.; Downs, H. H.; Rukavina, T. G. *J. Am. Chem. Soc.* **1974**, *96*, 5573.
(7) Buchanan, R. M.; Kessel, S. L.; Downs, H. H.; Pierpont, C. G.; Hendrickson, D. N. *J. Am. Chem. Soc.* **1978**, *100*, 7894.
(8) Pierpont, C. G.; Downs, H. H. *J. Am. Chem. Soc.* **1976**, *98*, 4834.

0002-7863/89/1511-2292$01.50/0

variable-temperature magnetic susceptibility measurements and Mössbauer spectroscopy on the iron complexes showed that the quinone ligands were in the semiquinone form, chelated to trivalent metal ions, $M^{III}(SQ)_3$.[7] Anomalous magnetic properties resulted from antiferromagnetic coupling between the radical ligands and the paramagnetic metal ions. Further reactions carried out with the neutral carbonyl complexes of Mn, Co, and Ni and 3,5-di-*tert*-butyl-1,2-benzoquinone produced the tetranuclear complexes $M_4(DBSQ)_8$ where, once again, radical semiquinones are coupled antiferromagnetically to the paramagnetic metal ions.[9-11] Octahedral $M(SQ)_3$ or oligomeric $M(SQ)_2$ complexes are now available for metals across the first transition series from vanadium[12] to copper.[13] All show metal-semiquinone antiferromagnetic coupling due to spin interactions between electrons in nonorthogonal orbitals, and correlations have been made between structural features and ligand charge. In recent studies, ferromagnetic metal-semiquinone coupling has been observed in compounds where spins are oriented in orthogonal orbitals.[14]

Continued study of the $Fe(CO)_5$ reaction with *o*-benzoquinones has shown that the form of the product obtained is dependent upon the relative proportions of iron carbonyl and quinone. In reactions carried out with excess quinone, the green tris(semiquinonate) product is obtained. With iron carbonyl present in excess, a dark blue product is formed that has a 2:1 quinone to iron ratio. This product obtained from reactions carried out with tetrachloro-1,2-benzoquinone is apparently polymeric from its low solubility. However, the bis(quinone) product obtained when 3,5-di-*tert*-butyl-1,2-benzoquinone is used was found to be more soluble and amenable to characterization. In this paper we report the structural characterization of both products obtained from the $Fe(CO)_5$-3,5-di-*tert*-butyl-1,2-benzoquinone reaction with the results of experiments that define charge distribution and magnetic properties.

Experimental Section

Physical Measurements. Electronic absorption measurements were made on a Cary 17 spectrophotometer.

Variable-temperature, solid-state magnetic susceptibility data were measured with a series 800 VTS-50 SQUID susceptometer (S.H.E. Corp.) maintained by the Physics Department at the University of Illinois. The susceptometer was operated at a magnetic field strength of 10 kG. Diamagnetic corrections were estimated from Pascal's constants and subtracted from the experimental susceptibility data to obtain the molar paramagnetic susceptibilities of the compounds. These molar paramagnetic susceptibilities were fit to the appropriate theoretical expressions by means of a least-squares-fitting computer program.[15]

^{57}Fe Mössbauer measurements were made on a constant-velocity-type instrument which has been described previously.[16] Mössbauer spectra were least-squares fit to Lorentzian line shapes. Isomer shift data are reported relative to that of iron foil at room temperature.

Compound Preparation. A crystalline sample of $Fe(DBSQ)_3$ was prepared by treating $Fe(CO)_5$ with a slight stoichiometric excess of 3,5-di-*tert*-butyl-1,2-benzoquinone (DBBQ) in toluene solution by the procedure described previously.[7] Slow evaporation of the solvent produced the crystalline sample used in this investigation.

$Fe_4(DBSQ)_4(DBCat)_4$. $Fe(CO)_5$, 1.0 mL (7.4 mmol) in 15 mL of toluene, was combined with 2.47 g (11.2 mmol) of DBBQ dissolved in 30 mL of toluene. The mixture was initially placed in an ice bath, since previous reactions had shown a tendency to bump violently upon heating. The reaction mixture was cautiously allowed to warm to room temperature and heated to reflux as reaction occurred. After 6 h the mixture was cooled. Crystals of the dark blue complex were obtained directly from the reaction in greater than 80% yield.

Table I. Crystal Data and Details of the Structure Determination and Refinement for $Fe(DBSQ)_3$ and $Fe_4(DBSQ)_4(DBCat)_4$

formula	$FeC_{42}H_{60}O_6$	$Fe_4C_{112}H_{160}O_{16}$
fw, g/mol	716.77	1985.87
space group[a]	$P2_1/n$	$P\bar{1}$
crystal system	monoclinic	triclinic
a,[b] Å	15.904 (3)	14.609 (3)
b, Å	15.891 (3)	14.779 (5)
c, Å	16.450 (4)	16.216 (5)
α, deg	90.00	118.06 (2)
β, deg	93.22 (2)	109.82 (3)
γ, deg	90.00	94.20 (2)
V, Å^3	4150 (1)	2789 (1)
D_{measd}, g/cm^3	1.14	1.40
D_{calcd}, g/cm^3	1.15	1.45
Z	4	1
$F(000)$	1567.96	1265.81
μ, cm^{-1}	3.76	8.31
diffractometer	Nicolet P3/F	
radiation, Å	Mo Kα (0.71073)	
graphite monochromator angle, deg	4.0	
temp, K	294-297	
cryst color	dark green	dark blue
cryst dimens, mm	0.81 × 0.76 × 0.61	0.40 × 0.09 × 0.07
scan technique	θ-2θ	
2θ, min-max, deg	3.0, 50.0	3.0, 45.0
indices scanned	±19h,+19k,±20l	±16h,±16k,±18l
scan speed, deg/min	3.91, 58.59	2.02, 58.59
scan range, deg/2θ	1.0° below Kα1 and 1.0° above Kα2	
no. of measd reflcns	14057	14547
no. of unique reflcns	7351	7329
no. of obsd reflcns	5054	3591
σ criterion	$F > 6\sigma(F)$	
absorp corrcn	empirical	
transm factors	0.971, 0.869	0.751, 0.666
method of phase detn	direct methods	
program	SHELXTL[d]	
scattering factors	neutral atoms[e]	
R and R_w (obsd data)[f]	0.050, 0.071	0.042, 0.055
weight	$1.0/(\sigma^2(F) + 0.0020F^2)$	
no. of params	469	597
ratio of observns to params	10.78	6.02
GOF	1.307	0.875

[a] *International Tables for X-ray Crystallography*; Kynoch Press: Birmingham, England, 1965; Vol. 1. [b] Cell dimensions were determined by least-squares fit of the setting angles for 25 reflections with 2θ in the range 32-38° for $Fe(DBSQ)_3$ and 10-23° for $Fe_4(DBSQ)_4(DBCAT)_4$. [c] By flotation methods in $ZnCl_2$. [d] Sheldrick, G. M. SHELXTL Plus, Version 2.1, 1987, and SHELXTL, Version 5.1, 1985, A Program For Crystal Structure Determination, Nicolet Analytical Instruments, Madison, WI 53711. [e] *International Tables for X-ray Crystallography*; Kynoch Press: Birmingham, England, 1974; Vol. 4. [f] The quantity minimized in the least-squares procedure is as follows: $\sum w(|F_o| - |F_c|)^2$. $R = \sum||F_o| - |F_c||/\sum|F_o|$; $R_w = [\sum w(|F_o| - |F_c|)^2/\sum w(F_o)^2]^{1/2}$.

Structure Determination on $Fe(DBSQ)_3$. Crystals of tris(3,5-di-*tert*-butyl-1,2-semiquinonato)iron(III) form as dark green parallelepipeds. A crystal of the complex suitable for crystallographic investigation was mounted and aligned on a Nicolet P3/F automated diffractometer. Two quadrants of data were collected, averaged in accord with the centrosymmetric, monoclinic space group (R_{av} = 0.035), and used for refinement. The structure was solved by direct methods; details of the structure determination and refinement are contained in Table I. Methyl carbon atoms of one *tert*-butyl group showed 2-fold disorder with half-atom occupancies at the two sites. Atom parameters are given in Table II. Carbon atoms C26-C28 and their primed equivalents were refined with half-occupancy factors.

Structure Determination on $Fe_4(DBSQ)_4(DBCat)_4$. Crystals of the (3,5-di-*tert*-butyl-1,2-semiquinonate)(3,5-di-*tert*-butylcatecholate)iron(III) tetranuclear complex form as dark blue rhombic needles. Data collection and structure determination were carried out with the parameters and procedure given in Table I. Photographs and reflection intensity measurements indicated that crystals of the complex diffracted

(9) Buchanan, R. M.; Pierpont, C. G. *Inorg. Chem.* **1979**, *18*, 3439.
(10) Lynch, M. W.; Buchanan, R. M.; Pierpont, C. G.; Hendrickson, D. N. *Inorg. Chem.* **1981**, *20*, 1038.
(11) Lynch, M. W.; Hendrickson, D. N.; Fitzgerald, B. J.; Pierpont, C. G. *J. Am. Chem. Soc.* **1984**, *106*, 2041.
(12) Cass, M. E.; Greene, D. L.; Buchanan, R. M.; Pierpont, C. G. *J. Am. Chem. Soc.* **1983**, *105*, 2680.
(13) Abakumov, G. A.; Lobanov, A. V.; Cherkasov, V. K.; Razuvaev, G. A. *Inorg. Chim. Acta* **1981**, *49*, 135.
(14) (a) Kahn, O.; Prins, R.; Reedijk, J.; Thompson, J. S. *Inorg. Chem.* **1987**, *26*, 3557. (b) Benelli, C.; Dei, A.; Gatteschi, D.; Pardi, L. *Inorg. Chem.* **1988**, *27*, 2831.
(15) Chandler, J. P. Program 66 of the Quantum Chemistry Program Exchange, Indiana University, Bloomington, IN.
(16) Cohn, M. J.; Timken, M. D.; Hendrickson, D. N. *J. Am. Chem. Soc.* **1984**, *106*, 6683.

Table II. Atomic Coordinates ($\times 10^4$) and Equivalent Isotropic Displacement Parameters ($Å^2 \times 10^3$) for $Fe(DBSQ)_3$

	x/a	y/b	z/c	U_{eq}[a]
Fe	2948 (1)	1833 (1)	6821 (1)	40 (1)
O1	1694 (1)	1847 (1)	6623 (1)	45 (1)
O2	2830 (1)	1626 (1)	5603 (1)	44 (1)
O3	3006 (1)	3097 (1)	6864 (1)	46 (1)
O4	4190 (1)	2037 (1)	6704 (1)	43 (1)
O5	2861 (1)	1649 (1)	8025 (1)	43 (1)
O6	3267 (1)	612 (1)	6926 (1)	45 (1)
C1	1427 (2)	1696 (2)	5886 (2)	36 (1)
C2	2073 (2)	1529 (2)	5318 (2)	39 (1)
C3	1839 (2)	1274 (2)	4504 (2)	43 (1)
C4	995 (2)	1279 (2)	4291 (2)	46 (1)
C5	346 (2)	1509 (2)	4825 (2)	41 (1)
C6	573 (2)	1699 (2)	5610 (2)	41 (1)
C7	2521 (2)	1016 (2)	3942 (2)	54 (1)
C8	3083 (3)	1776 (3)	3773 (3)	77 (2)
C9	2131 (3)	673 (4)	3130 (2)	98 (2)
C10	3061 (3)	311 (3)	4331 (3)	73 (2)
C11	−564 (2)	1518 (2)	4484 (2)	52 (1)
C12	−638 (3)	2114 (3)	3762 (3)	90 (2)
C13	−1172 (3)	1815 (4)	5104 (3)	112 (3)
C14	−821 (3)	644 (3)	4191 (3)	97 (2)
C15	3727 (2)	3411 (2)	6728 (2)	39 (1)
C16	4398 (2)	2809 (2)	6618 (2)	36 (1)
C17	5225 (2)	3090 (2)	6440 (2)	40 (1)
C18	5336 (2)	3943 (2)	6419 (2)	44 (1)
C19	4681 (2)	4555 (2)	6541 (2)	42 (1)
C20	3898 (2)	4281 (2)	6688 (2)	45 (1)
C21	5909 (2)	2448 (2)	6281 (2)	54 (1)
C22	6093 (2)	1906 (2)	7044 (3)	68 (1)
C23	5600 (3)	1880 (3)	5563 (3)	72 (2)
C24	6724 (2)	2868 (3)	6055 (3)	77 (2)
C25	4898 (2)	5495 (2)	6532 (2)	50 (1)
C26	4960 (7)	5781 (7)	7451 (7)	83 (4)
C26′	5323 (12)	5702 (10)	5702 (8)	97 (7)
C27	5753 (6)	5669 (6)	6173 (8)	99 (5)
C27′	5480 (11)	5712 (11)	7241 (11)	100 (7)
C28	4221 (7)	5996 (7)	6082 (7)	85 (4)
C28′	4039 (12)	6061 (11)	6541 (13)	102 (8)
C29	3133 (2)	928 (2)	8280 (2)	39 (1)
C30	3403 (2)	355 (2)	7656 (2)	38 (1)
C31	3786 (2)	−431 (2)	7879 (2)	42 (1)
C32	3778 (2)	−640 (2)	8684 (2)	44 (1)
C33	3459 (2)	−115 (2)	9303 (2)	44 (1)
C34	3158 (2)	662 (2)	9099 (2)	43 (1)
C35	4165 (2)	−972 (2)	7228 (2)	53 (1)
C36	4786 (3)	−446 (2)	6753 (3)	72 (2)
C37	3463 (3)	−1306 (3)	6639 (2)	73 (2)
C38	4653 (3)	−1715 (2)	7599 (3)	75 (2)
C39	3432 (2)	−472 (2)	10169 (2)	55 (1)
C40	2772 (3)	−1167 (3)	10140 (3)	98 (2)
C41	4256 (3)	−875 (4)	10454 (3)	105 (2)
C42	3215 (4)	185 (3)	10774 (2)	125 (3)

[a] U_{eq} defined as one-third of the trace of the orthogonalized u_{ij} tensor.

poorly. A sphere of data was collected to a 2θ value of 45°, related reflections were averaged in accord with the centrosymmetric, triclinic space group ($R_{av} = 0.041$), and the averaged data set was used in the structure determination and refinement. Structure determination showed that the complex molecule is tetranuclear and located about a crystallographic inversion center. Atom parameters are given in Table III.

Tables containing anisotropic thermal parameters, hydrogen atom positions, and structure factors for both structure determinations are available as supplementary material.

Results

The electronic structure of complexes containing unsaturated five-membered chelate rings has long been a subject of interest.[17] Delocalization within the chelate rings of complexes containing 1,2-dithiolene and 1,2-diimine ligands makes the formal assignment of charge to ligand and metal inappropriate. This was found to be particularly true for the neutral 1,2-dithiolene complexes, $M(S_2C_2R_2)_n$, $n = 2, 3$, and for the neutral diimine complex bis(*o*-phenylenediimine)nickel.[18] The neutral complexes prepared

Table III. Atomic Coordinates ($\times 10^4$) and Isotropic Displacement Parameters ($Å^2 \times 10^3$) for $Fe_4(DBSQ)_4(DBCat)_4$

	x/a	y/b	z/c	U_{eq}[a]
Fe1	1687 (1)	284 (1)	−590 (1)	42 (1)
Fe2	389 (1)	−852 (1)	250 (1)	36 (1)
O1	1838 (2)	−140 (3)	544 (3)	34 (2)
O2	1202 (3)	−568 (3)	1655 (3)	44 (2)
C1	2533 (4)	118 (4)	1442 (4)	35 (3)
C2	2153 (4)	−151 (4)	2047 (4)	37 (3)
C3	2839 (4)	72 (5)	3027 (4)	49 (4)
C4	3830 (5)	521 (5)	338 (4)	56 (4)
C5	4212 (4)	807 (4)	2771 (4)	45 (4)
C6	3556 (4)	598 (4)	1832 (4)	42 (3)
C7	2438 (5)	−218 (5)	3670 (5)	71 (5)
C8	1640 (5)	354 (6)	3876 (5)	89 (5)
C9	3290 (6)	128 (8)	4708 (5)	120 (7)
C10	1986 (6)	−1415 (6)	3076 (6)	110 (7)
C11	5354 (4)	1320 (5)	3213 (5)	61 (4)
C12	5791 (5)	2181 (6)	4348 (6)	103 (6)
C13	5594 (5)	1748 (9)	2624 (7)	173 (11)
C14	5868 (5)	448 (7)	3110 (6)	107 (6)
O3	1080 (2)	1404 (3)	64 (3)	39 (2)
O4	−259 (3)	2333 (3)	464 (3)	43 (2)
C15	1394 (4)	2505 (4)	609 (4)	37 (3)
C16	653 (4)	2988 (4)	810 (4)	40 (3)
C17	868 (4)	4104 (4)	1364 (4)	43 (3)
C18	1855 (4)	4656 (4)	1677 (4)	51 (4)
C19	2604 (4)	4194 (4)	1495 (4)	44 (3)
C20	2357 (4)	3079 (4)	945 (4)	42 (3)
C21	76 (5)	4662 (5)	1614 (6)	65 (5)
C22	501 (5)	5885 (5)	2271 (6)	100 (6)
C23	−297 (5)	4305 (5)	2225 (5)	80 (5)
C24	−828 (5)	4341 (5)	591 (6)	82 (5)
C25	3678 (4)	4879 (4)	1881 (5)	54 (4)
C26	3955 (5)	5925 (6)	2847 (7)	139 (7)
C27	3708 (6)	5065 (8)	1061 (7)	156 (9)
C28	4489 (4)	4346 (6)	2094 (6)	101 (6)
O5	47 (2)	−566 (3)	−926 (2)	37 (2)
O6	1289 (3)	−1016 (3)	−1802 (3)	49 (2)
C29	−355 (4)	−1421 (4)	−1938 (4)	37 (3)
C30	327 (4)	−1627 (4)	−2390 (4)	40 (3)
C31	−6 (4)	−2445 (4)	−3420 (4)	47 (3)
C32	−1019 (4)	−3054 (4)	−3938 (4)	51 (3)
C33	−1695 (4)	−2882 (4)	−3484 (4)	43 (3)
C34	−1344 (4)	−2045 (4)	−2466 (4)	39 (3)
C35	702 (5)	−2672 (5)	−3970 (5)	66 (4)
C36	1561 (5)	−3006 (6)	−3431 (6)	95 (5)
C37	1134 (5)	−1659 (6)	−3916 (5)	94 (5)
C38	167 (6)	−3561 (6)	−5100 (5)	107 (5)
C39	−2769 (4)	−3644 (5)	−4139 (4)	53 (4)
C40	−3415 (4)	−3344 (5)	−3536 (5)	83 (5)
C41	−2730 (5)	−4761 (5)	−4441 (7)	113 (6)
C42	−3282 (5)	−3573 (7)	−5075 (6)	128 (7)
O7	3161 (3)	682 (3)	−83 (3)	46 (2)
O8	1901 (3)	1072 (3)	−1329 (3)	49 (2)
C43	3544 (4)	1179 (4)	−424 (4)	43 (3)
C44	2825 (4)	1394 (4)	−1134 (4)	45 (3)
C45	3185 (4)	1992 (4)	−1513 (4)	48 (4)
C46	4208 (4)	2316 (5)	−1131 (5)	58 (4)
C47	4935 (4)	2108 (4)	−448 (4)	48 (4)
C48	4588 (4)	1527 (4)	−106 (4)	49 (4)
C49	2440 (5)	2208 (6)	−2265 (5)	64 (5)
C50	1781 (6)	2847 (6)	−1798 (6)	97 (6)
C51	1745 (6)	1155 (6)	−3243 (5)	91 (5)
C52	2987 (6)	2843 (7)	−2572 (7)	115 (7)
C53	6061 (4)	2582 (5)	−75 (5)	63 (4)
C54	6719 (5)	2177 (7)	552 (6)	98 (6)
C55	6312 (5)	3809 (5)	598 (6)	91 (5)
C56	6303 (5)	2273 (5)	−1010 (5)	83 (5)

[a] U_{eq} defined as one-third of the trace of the orthogonalized U_{ij} tensor.

(17) (a) McCleverty, J. A. *Prog. Inorg. Chem.* **1968**, *10*, 49. (b) Eisenberg, R. *Prog. Inorg. Chem.* **1970**, *12*, 295.

(18) (a) Balch, A. L.; Holm, R. H. *J. Am. Chem. Soc.* **1966**, *88*, 5201. (b) Hall, G. S.; Soderberg, R. H. *Inorg. Chem.* **1968**, *7*, 2300.

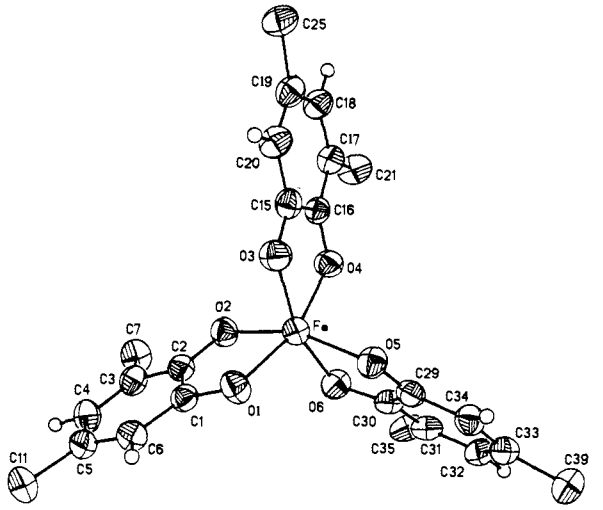

Figure 1. View of the $Fe(DBSQ)_3$ molecule.

with the *o*-quinone ligands offer the same possibility for chelate ring delocalization. In cases where there is a single unpaired electron, EPR can provide information on the electronic ground state. Weak coupling to the ^{51}V nuclei of the neutral tris(semiquinonate)vanadium(III) complexes[12] and strong coupling to the rhenium nuclei of the tris(catecholate)rhenium(VI) complexes[19] showed little evidence of delocalization, in marked contrast to their 1,2-dithiolene analogues. Mössbauer spectroscopy is available as a spectroscopic tool that may be used to assign metal ion oxidation state in complexes of iron. Clear differences appear in the spectra of complexes containing high- and low-spin ferric and ferrous ions, and Mössbauer spectra recorded in the presence of a strong magnetic field can be used to examine the internal ^{57}Fe hyperfine field. The latter technique has been used to show that the unusual magnetic properties of complexes containing ferric iron chelated by semiquinone ligands arise from antiferromagnetic coupling between the high-spin metal ion and the paramagnetic organic ligands.[20] Specific systems included in this investigation were the $Fe^{III}(L)(SQ)$ and $Fe^{III}(L)(Cat)(SQ)$ complexes with $S = 2$ ground states and the $Fe^{III}(SQ)_3$ complexes with $S = 1$ ground states.

The procedure used in the synthesis of the neutral $Fe(SQ)_3$ complexes involves treating $Fe(CO)_5$ with the *o*-benzoquinone form of the semiquinone ligand. It was noted that in reactions carried out using a stoichiometry of iron to quinone that was less than 1:3 with either tetrachloro-1,2-benzoquinone or 3,5-di-*tert*-butyl-1,2-benzoquinone a dark blue product formed, rather than the dark green $Fe(SQ)_3$ complexes characterized previously.[7] Chemical analyses indicated that the products formed with two quinone ligands per iron, $Fe(Q)_2$. The insolubility of the product obtained with tetrachlorobenzoquinone has prevented detailed characterization. However, the product obtained with DBBQ proved to be somewhat more soluble and amenable to characterization in dilute solution. The complex shows strong electronic absorption bands at 392 (ϵ = 14000 M^{-1} cm^{-1}) and 680 (10000) nm in the UV–vis (toluene), in contrast to bands at 376 (22000), 430 (10000), and 650 (17000) nm for $Fe(DBSQ)_3$. Furthermore, addition of DBBQ to a toluene solution of the complex was observed to produce $Fe(DBSQ)_3$. For a complex containing two quinone-derived ligands per iron there are two reasonable charge distributions possible. Related reactions carried out with the carbonyls of Mn, Co, and Ni gave tetranuclear products containing divalent metals and semiquinone ligands, $[M^{II}(DBSQ)_2]_4$, M = Mn, Co, Ni.[9,11] By analogy, the iron complex could be of similar structure and charge distribution as $[Fe^{II}(DBSQ)_2]_4$. A charge distribution with mixed-charge ligands and high-spin ferric iron is also a possibility. Mössbauer spectra of bis(quinone)iron complexes containing nitrogen-donor ligands indicated that the metal was ferric iron, and that $Fe^{III}(bpy)(DBSQ)(DBCat)$ and related complexes contained mixed-charge quinone ligands.[21] The delocalized electronic structures of the 1,2-dithiolene complexes suggest a variant of this second possibility wherein the electronic structure is delocalized over both ligand and metal. To investigate these possibilities the bis(3,5-di-*tert*-butylquinone)iron complex has been characterized structurally, magnetically, and by using Mössbauer spectroscopy. For comparison, the structure of tris(3,5-di-*tert*-butylsemiquinonate)iron(III) has also been determined.

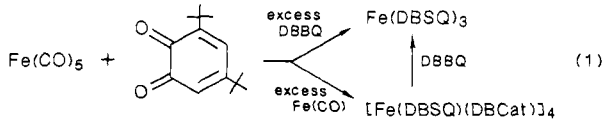

(1)

Table IV. Selected Bond Lengths (Å) and Angles (deg) for $Fe(DBSQ)_3$

	Fe–O Lengths		
Fe–O1	2.004 (2)	Fe–O2	2.028 (2)
Fe–O3	2.012 (2)	Fe–O4	2.021 (2)
Fe–O5	2.015 (2)	Fe–O6	2.010 (2)
	Fe–O Angles		
O2–Fe–O1	78.7 (1)	O3–Fe–O1	92.1 (1)
O3–Fe–O2	101.4 (1)	O4–Fe–O1	162.2 (1)
O4–Fe–O2	88.2 (1)	O4–Fe–O3	78.5 (1)
O5–Fe–O1	92.2 (1)	O5–Fe–O2	160.0 (1)
O5–Fe–O3	96.6 (1)	O5–Fe–O4	103.8 (1)
O6–Fe–O1	105.6 (1)	O6–Fe–O2	86.4 (1)
O6–Fe–O3	161.8 (1)	O6–Fe–O4	85.4 (1)
O6–Fe–O5	78.9 (1)		
	Ligand 1 Lengths		
O1–C1	1.284 (3)	O2–C2	1.277 (3)
C1–C2	1.451 (4)	C1–C6	1.408 (4)
C2–C3	1.428 (4)	C3–C4	1.368 (4)
C3–C7	1.520 (4)	C4–C5	1.438 (4)
C5–C6	1.355 (4)	C5–C11	1.523 (4)
	Ligand 1 Angles		
C1–O1–Fe	115.1 (2)	C2–O2–Fe	114.6 (2)
C2–C1–O1	115.8 (2)	C6–C1–O1	124.4 (3)
C6–C1–C2	119.8 (3)	C1–C2–O2	115.3 (3)
C3–C2–O2	124.8 (3)	C3–C2–C1	119.9 (3)
	Ligand 2 Lengths		
O3–C15	1.281 (3)	O4–C16	1.281 (3)
C15–C16	1.451 (4)	C15–C20	1.412 (4)
C16–C17	1.434 (4)	C17–C18	1.368 (4)
C17–C21	1.525 (4)	C18–C19	1.446 (4)
C19–C20	1.353 (4)	C19–C25	1.535 (4)
	Ligand 2 Angles		
C15–O3–Fe	114.9 (2)	C16–O4–Fe	115.1 (2)
C16–C15–O3	115.9 (3)	C20–C15–O3	124.5 (3)
C20–C15–C16	119.6 (3)	C15–C16–O4	114.9 (3)
C17–C16–O4	124.4 (3)	C17–C16–C15	120.7 (3)
	Ligand 3 Lengths		
O5–C29	1.287 (3)	O6–C30	1.276 (3)
C29–C30	1.455 (4)	C29–C34	1.410 (4)
C30–C31	1.428 (4)	C31–C32	1.365 (4)
C31–C35	1.525 (4)	C32–C33	1.431 (4)
C33–C34	1.360 (4)	C33–C39	1.536 (4)
	Ligand 3 Angles		
C29–O5–Fe	114.1 (2)	C30–O6–Fe	114.8 (2)
C30–C29–O5	115.8 (3)	C34–C29–O5	124.6 (3)
C34–C29–C30	119.6 (3)	C29–C30–O6	115.0 (3)
C31–C30–O6	124.8 (3)	C31–C30–C29	120.3 (3)

Structure of Tris(3,5-di-*tert*-butylsemiquinonate)iron(III). The molecular structure of $Fe(DBSQ)_3$ consists of an octahedrally coordinated metal ion with chelated semiquinone ligands in a

(19) deLearie, L. A.; Haltiwanger, R. C.; Pierpont, C. G. *Inorg. Chem.* **1987**, *26*, 817.

(20) Cohn, M. J.; Xie, C.-L.; Tuchagues, J.-P.; Pierpont, C. G.; Hendrickson, D. N. *J. Am. Chem. Soc.*, submitted for publication.

(21) Lynch, M. W.; Valentine, M.; Hendrickson, D. N. *J. Am. Chem. Soc.* **1982**, *104*, 6982.

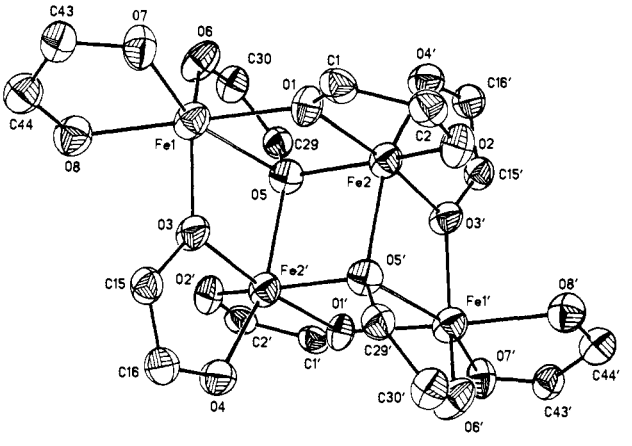

Figure 2. View of the inner core of the centrosymmetric $Fe_4(DBSQ)_4(DBCat)_4$ molecule. Structural features indicate that ligands containing oxygens O1, O2 and O7, O8 are semiquinone and ligands containing O3, O4 and O5, O6 are catecholate.

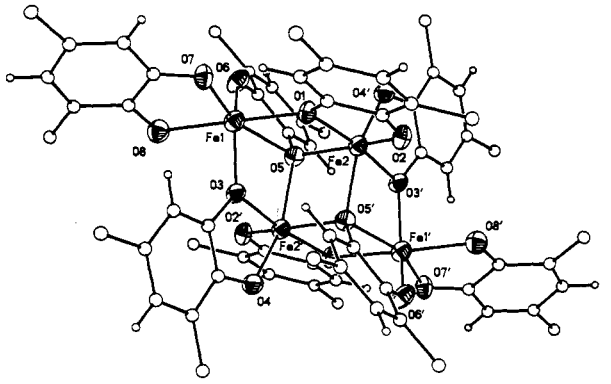

Figure 3. View of the $Fe_4(DBSQ)_4(DBCat)_4$ molecule. *tert*-Butylmethyl carbon atoms have been omitted.

molecule of C_3 symmetry. A view of the molecule is shown in Figure 1; bond distances and angles are given in Table IV. The mean Fe–O length is 2.015 (2) Å, a value that compares well with other bond lengths of trischelated ferric iron complexes with oxygen donor ligands. The tris(catecholato)iron(III) anion has been reported to have a length of 2.015 (6) Å,[22] and the semiquinone complex tris(9,10-phenanthrenesemiquinonate)iron(III) has an Fe–O bond length of 2.027 (4) Å.[7] Detailed features of the three independent 3,5-di-*tert*-butylsemiquinone ligands show extraordinary consistency. Carbon–oxygen bond lengths average to 1.281 (3) Å, typical of values found for other semiquinone structures, and carbon–carbon lengths also show a characteristic pattern. The longest C–C length of the ring is found for the C1–C2 bond, and the shortest lengths are found for the C3–C4 and C5–C6 bonds. These would be double bonds in the benzoquinone form of the ligand. The electronic effect of the *tert*-butyl substituents is found in the small but consistent difference between lengths of the C2–C3 and C1–C6 bonds. Tert-Butyl substituents at the 3-positions of the ligand rings are directed at the same triangular face of the octahedron, giving an isomer of C_3 symmetry, rather than the asymmetric isomer with only two 3-*tert*-butyl substituents directed at one face. Structures have now been reported for $Fe(DBSQ)_3$, $Cr(DBSQ)_3$,[23] $V(DBCat)_3^-$,[24] $Os(DBCat)_3$,[25] and $Re(DBCat)_3$.[19] All but the Os complex form

(22) Raymond, K. N.; Isied, S. S.; Brown, L. D.; Fronczek, F. R.; Nibert, J. H. *J. Am. Chem. Soc.* **1976**, *98*, 1767.
(23) Sofen, S. R.; Ware, D. C.; Cooper, S. R.; Raymond, K. N. *Inorg. Chem.* **1979**, *18*, 234.
(24) Cass, M. E.; Gordon, N. R.; Pierpont, C. G. *Inorg. Chem.* **1986**, *25*, 3962.
(25) Nielson, A. J.; Griffith, W. P. *J. Chem. Soc., Dalton Trans.* **1978**, 1501.

Table V. Selected Bond Lengths (Å) and Angles (deg) for $Fe_4(DBSQ)_4(DBCat)_4$

	Fe–O Lengths[a]		
Fe1–Fe2	3.421 (1)	Fe1–Fe2′	3.358 (1)
Fe2–Fe2′	3.161 (1)	Fe2–O5′	2.122 (4)
Fe1–O1	2.156 (5)	Fe1–O3	1.963 (4)
Fe1–O5	2.377 (4)	Fe1–O6	1.844 (3)
Fe1–O7	1.954 (4)	Fe1–O8	2.100 (5)
Fe2–O1	2.082 (4)	Fe2–O2	1.993 (4)
Fe2–O5	2.050 (5)	Fe2–O3′	2.036 (4)
Fe2–O4′	1.891 (4)		
	Fe–O Angles		
O1–Fe1–O3	89.9 (2)	O1–Fe1–O5	71.5 (1)
O3–Fe1–O5	72.2 (1)	O1–Fe1–O6	103.7 (2)
O3–Fe1–O6	138.1 (1)	O5–Fe1–O6	75.1 (2)
O1–Fe1–O7	89.5 (2)	O3–Fe1–O7	117.1 (1)
O5–Fe1–O7	159.3 (2)	O6–Fe1–O7	102.6 (2)
O1–Fe1–O8	163.3 (1)	O3–Fe1–O8	85.8 (2)
O5–Fe1–O8	122.1 (1)	O6–Fe1–O8	90.1 (2)
O7–Fe1–O8	78.1 (2)	O1–Fe2–O2	78.3 (2)
O1–Fe2–O5	79.9 (2)	O2–Fe2–O5	155.0 (2)
O1–Fe2–O3′	173.0 (2)	O2–Fe2–O3′	105.4 (2)
O5–Fe2–O3′	95.1 (2)	O1–Fe2–O4′	104.4 (2)
O2–Fe2–O4′	96.1 (2)	O5–Fe2–O4′	101.1 (2)
O3′–Fe2–O4′	81.3 (2)	O1–Fe2–O5′	97.7 (1)
O2–Fe2–O5′	89.4 (2)	O5–Fe2–O5′	81.5 (2)
O3′–Fe2–O5′	76.7 (1)	O4′–Fe2–O5′	157.9 (2)
	Ligand 1 Lengths		
O1–C1	1.310 (6)	O2–C2	1.272 (7)
C1–C2	1.462 (11)	C1–C6	1.385 (8)
C2–C3	1.419 (9)	C3–C4	1.357 (9)
C3–C7	1.553 (13)	C4–C5	1.420 (12)
C5–C6	1.362 (9)	C5–C11	1.538 (8)
	Ligand 1 Angles		
Fe1–O1–Fe2	107.6 (1)	Fe1–O1–C1	136.8 (4)
Fe2–O1–C1	113.6 (4)	Fe2–O2–C2	116.9 (5)
O1–C1–C2	114.4 (5)	O1–C1–C6	125.8 (7)
C2–C1–C6	119.8 (5)	O2–C2–C1	116.6 (5)
O2–C2–C3	123.8 (7)	C1–C2–C3	119.6 (5)
	Ligand 2 Lengths		
O3–C15	1.378 (6)	O4–C16	1.350 (7)
C15–C16	1.387 (9)	C15–C20	1.366 (8)
C16–C17	1.402 (7)	C17–C18	1.394 (9)
C17–C21	1.525 (10)	C18–C19	1.375 (9)
C19–C20	1.398 (8)	C19–C25	1.544 (8)
	Ligand 2 Angles		
Fe1–O3–C15	133.8 (4)	Fe1–O3–Fe2′	114.2 (1)
C15–O3–Fe2′	111.5 (3)	C16–O4–Fe2′	116.3 (3)
O3–C15–C16	114.2 (5)	O3–C15C20	123.4 (5)
C16–C15–C20	122.4 (5)	O4–C16–C15	116.7 (5)
O4–C16–C17	122.9 (5)	C15–C16–C17	120.5 (5)
	Ligand 3 Lengths		
O5–C29	1.387 (5)	O6–C30	1.340 (6)
C29–C30	1.396 (6)	C29–C34	1.377 (7)
C30–C31	1.397 (7)	C31–C32	1.398 (8)
C31–C35	1.541 (11)	C32–C33	1.391 (10)
C33–C34	1.389 (7)	C33–C39	1.531 (7)
	Ligand 3 Angles		
Fe1–O5–Fe2	100.9 (1)	Fe1–O5–C29	105.4 (4)
Fe2–O5–C29	119.5 (4)	Fe1–O5–Fe2′	96.4 (1)
Fe2–O5–Fe2′	98.5 (2)	C29–O5–Fe2′	130.4 (3)
Fe1–O6–C30	123.6 (4)	O5–C29–C30	115.1 (4)
O5–C29–C34	123.3 (6)	C30–C29–C34	121.6 (4)
O6–C30–C29	117.6 (4)	O6–C30–C31	122.5 (6)
C29–C30–C31	119.9 (5)		
	Ligand 4 Lengths		
O7–C43	1.302 (9)	O8–C44	1.274 (7)
C43–C44	1.450 (9)	C43–C48	1.398 (8)
C44–C45	1.448 (12)	C45–C46	1.355 (8)
C45–C49	1.512 (11)	C46–C47	1.421 (10)
C47–C48	1.371 (12)	C47–C53	1.524 (9)
	Ligand 4 Angles		
Fe1–O7–C43	117.1 (4)	Fe1–O8–C44	113.9 (4)
O7–C43–C44	116.0 (5)	O7–C43–C48	122.8 (6)
C44–C43–C48	121.2 (7)	O8–C44–C43	114.8 (7)
O8–C44–C45	125.1 (6)	C43–C44–C45	119.9 (5e

[a] Displacement of O5 from the Fe1, Fe2, Fe2′ plane, 1.047 (3) Å.

Table VI. Mössbauer Least-Squares Fitting Parameters for Iron–Semiquinone Complexes

	T, K	δ,[a] mm/s	ΔE_Q, mm/s
$Fe^{III}(DBSQ)_3$	90	0.559 (2)	0.752 (2)
$Fe^{III}(bpy)(DBSQ)(DBCat)$	295	0.477 (3)	1.092 (6)
	4.2	0.558 (1)	1.104 (1)
$Fe^{III}_4(DBSQ)_4(DBCat)_4$	90	0.4758 (8)	1.326 (2) inner
		0.4852 (8)	1.749 (2) outer

[a] Isomer shift versus iron foil at room temperature.

in the C_3 isomeric form, and molecular mechanics calculations indicate a slight preference for the C_3 isomer over the C_1 isomer. The structural features of $Cr(DBSQ)_3$ are quite similar to those of $Fe(DBSQ)_3$. However, the Cr complex crystallizes in the acentric rhombohedral space group $R3$, with molecules located about sites of 3-fold symmetry, and with spontaneous resolution of complex molecules in the form of the Λ-cis isomer.[23]

Structure of Tetrakis(3,5-di-*tert*-butylsemiquinato)tetrakis(3,5-di-*tert*-butylcatecholato)tetrairon(III). The molecular structure of the bis(quinone)iron complex is tetranuclear with features that clearly indicate localized semiquinone and catecholate coordination to high-spin ferric iron. Views of the $Fe_4(DBSQ)_4(DBCat)_4$ molecule are shown in Figures 2 and 3; bond distances and angles are given in Table V. Gross features of the centrosymmetric molecule are similar to those of $Mn_4(DBSQ)_8$ and $Co_4(DBSQ)_8$.[9,11] Three different ligand environments are found in $Fe_4(DBSQ)_4(DBCat)_4$. Two quinone ligands chelate to the Fe1 centers, two chelate to Fe1 but also bridge to two centrosymmetrically related Fe2 centers, and four chelate to the two Fe2 ions and bridge to an adjacent Fe1. Examination of ligand structural features shows that the oxygen atoms O3–O4 and O5–O6 are associated with catecholate ligands, while O1–O2 and O7–O8 are semiquinone. Each iron of the molecule is chelated by one semiquinone and one catecholate, and it is reasonable to view the molecule as an assembly of four Fe(DBSQ)(DBCat) units. The inversion center requires that the Fe_4 core be perfectly planar, ostensibly consisting of two coplanar Fe_3 triangles sharing a common Fe2–Fe2′ edge. Catecholate oxygen atoms O5 and O5′ sit atop the two triangular units in much the same way that oxo ligands bridge the triiron core of the basic iron acetates, $Fe_3O(Ac)_6L_3$. The Fe_4O_2 unit appears commonly in tetranuclear iron complexes[26] and the planar $Fe_4(OH)_2$ unit containing hydroxo ligands, which are more electronically similar to the catecholate oxygens, is found in various mineral structures.[27]

Detailed features of $Fe^{III}_4(DBSQ)_4(DBCat)_4$ show marked similarity to $Mn^{II}_4(DBSQ)_8$, which also contains a high-spin d^5 metal ion, with allowance for the 0.18-Å decreases in radius of Fe^{3+} relative to Mn^{2+}. Iron–iron separations within the Fe_3 triangles range from 3.161 (1) to 3.421 (1) Å compared with values of from 3.298 (4) to 3.565 (3) Å for the manganese tetramer. In both cases the shortest lengths occur for the inner centrosymmetrically related metals M2 and M2′. Structural features of the semiquinone and catecholate ligands reflect the electronic difference. Catecholate ligands O3–O4 and O5–O6 have C–O lengths of 1.350 (7) and 1.340 (6) Å to oxygens O4 and O6, which bond terminally to one metal, with longer values of 1.378 (6) and 1.387 (5) Å to oxygens O3 and O5, which bridge to one and two metals, respectively. Ring C–C lengths are typical of values reported for aromatic phenyl rings. The semiquinone ligands have shorter C–O lengths, as expected. Lengths to oxygens O2 and O8 have values of 1.272 (7) and 1.274 (7) Å, the length to O7 is slightly longer, 1.302 (9) Å, perhaps due to the strong Fe1–O7 bond, and the C–O length to bridging oxygen O1 is 1.310 (6) Å. Ring C–C lengths show the same pattern found for the semiquinone ligands of $Fe(DBSQ)_3$. The longest values are found for the C1–C2 bonds, the shortest are the C3–C4 and C5–C6 bonds, and the C2–C3 bond is slightly longer than the C1–C6 bond.

(26) Gorun, S. M.; Lippard, S. J. *Inorg. Chem.* **1988**, *27*, 149.
(27) (a) Moore, P. B. *Am. Mineral.* **1972**, *57*, 397. (b) Kampf, A. R.; Moore, P. B. *Am. Mineral.* **1977**, *62*, 60.

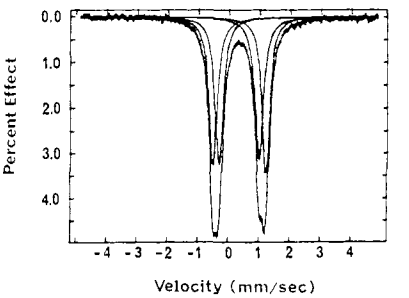

Figure 4. ^{57}Fe Mössbauer spectrum of $Fe_4(DBSQ)_4(DBCat)_4$ at 100 K. The solid lines show the result of least-squares fitting the spectrum to two equal-area quadrupole-split doublets.

Oxygen–iron bond lengths of $Fe_4(DBSQ)_4(DBCat)_4$ follow the general pattern of lengths found for $Mn_4(DBSQ)_8$. Detailed comparison of catecholate and semiquinone Fe–O lengths shows that catecholate lengths tend to be slightly shorter. This is apparent at Fe2, where both chelated ligands bridge to one adjacent metal and oxygens of the catecholate (O3, O4) and semiquinone (O1, O2) are in comparable coordination sites. Catecholate lengths are shorter than the semiquinone lengths at equivalent positions. In both the Mn and Fe structures, the triply bridging oxygen is located toward the Fe2–Fe2′ edge of the iron triangle with the Fe1–O5 length as the longest Fe–O length of the structure. Ignoring O5, there is a clear distortion in the coordination geometry about Fe1 toward a trigonal bipyramid with O1 and O8 occupying axial sites as reflected in the bond angles about the metal. Catecholate oxygen O6 is bonded at an equatorial site, and the Fe1–O6 length of the chelate ring is the shortest length of the structure.

In general, structural features within the Fe_4O_{16} core resemble those of $Mn_4(DBSQ)_8$ with allowance for the difference in metal ion radius and for slightly shorter lengths to the catecholate oxygens.

Mössbauer Spectra. Mössbauer spectra have been reported previously for $Fe(DBSQ)_3$ and for $Fe(N–N)(DBSQ)(DBCat)$.[7,21] Isomer shift and quadrupole-splitting values for these complexes are given in Table VI. We have also recorded Mössbauer spectra at high magnetic field to measure the internal ^{57}Fe hyperfine field. These studies have indicated that the metal ions are indeed high-spin ferric iron and that anomalies in their magnetic properties arise from antiferromagnetic coupling between the $S = {}^5/_2$ metal ion and the $S = {}^1/_2$ semiquinone ligands.[20] The Mössbauer spectrum of $Fe_4(DBSQ)_4(DBCat)_4$ is shown in Figure 4. The spectrum has been fit to two quadrupole-split doublets of equal area with isomer shift values of 0.4758 (8) and 0.4852 (8) mm/s (vs iron foil) and quadrupole-splitting parameters of 1.326 (2) and 1.749 (2) mm/s, respectively. These values are quite in accord with Mössbauer parameters commonly associated with high-spin ferric ion and agree well with values recorded for other Fe(III)–semiquinone complexes given in the table.

Magnetic Susceptibility. Iron–semiquinone antiferromagnetic exchange within the $Fe^{III}(SQ)_3$ complexes was observed to be weaker for the 9,10-phenanthrenesemiquinone and tetrachloro-1,2-semiquinone ligands than for 3,5-di-*tert*-butylsemiquinone.[7] The magnetic moment of $Fe(DBSQ)_3$ was observed to be temperature independent, with a value of 2.95 μ_B (285 K) reflecting the $S = 1$ ground state. Related complexes prepared with the other two quinone ligands show temperature-dependent magnetic moments indicating thermal population of excited ($S > 1$) spin states and weaker Fe(III)–SQ coupling. The magnetic properties of the Fe(N–N)(DBSQ)(DBCat) complexes would be expected to reflect the $S = 2$ ground state arising from strong Fe–SQ coupling. The 286 K magnetic moment of Fe(bpy)(DBSQ)(DBCat) is 5.19 μ_B in accord with this spin state, but as temperature was decreased, the magnetic moment dropped to 0.49 μ_B at 4.2 K. This led to the conclusion that certain of these complexes were oligomeric.[21]

Magnetic susceptibility measurements on $Fe_4(DBSQ)_4(DBCat)_4$ were recorded as a function of temperature. A plot of μ_{eff} versus

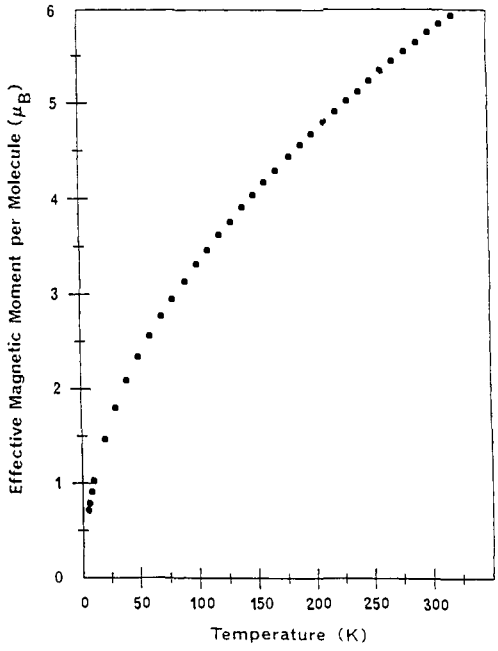

Figure 5. Plot of effective magnetic moment per $Fe_4(DBSQ)_4(DBCat)_4$ molecule versus temperature.

temperature is shown in Figure 5. The magnetic moment per Fe_4 molecule at 321 K was found to be 5.94 μ_B and μ_{eff} decreases with temperature to a value of 0.72 μ_B per molecule at 5.0 K. With an $S = 2$ resultant spin per Fe(DBSQ)(DBCat) unit of the molecule, this magnetic behavior requires coupling between iron centers as well as iron–semiquinone coupling. From the magnetic behavior of the other Fe–DBSQ complexes and that of oxo-bridged Fe(III) tetramers it seems reasonable to assume that Fe–DBSQ coupling is stronger than Fe–O–Fe coupling, and that the temperture dependence of magnetic moment is due primarily to the Fe–O–Fe coupling propagated through the semiquinone and catecholate oxygen atom bridges. With the different types of magnetic interactions present in this low-symmetry molecule, a theoretical model is virtually impossible to derive.

Discussion

The quinone ligands are unique in their ability to form stable complexes with ligands of mixed charge. Similar behavior has been attributed to bipyridine in the photoexcited state of $Ru(bpy)_3^{2+}$. However, the bipyridyl radical anion is far more reactive than coordinated semiquinone, and with the short excited-state lifetime of the complex, characterization of this charge distribution for bipyridine has been difficult.[5a] Mixed-charge quinone ligands have been characterized structurally in Co(bpy)(DBSQ)(DBCat),[28] $[VO(DBSQ)(DBCat)]_2$,[12] and now in $Fe_4(DBSQ)_4(DBCat)_4$. Spectroscopic and magnetic properties together with structural features of the metal ions verify the mixed-charge-ligand charge distribution, and structural features of the quinones show clear differences for the "valence-trapped" semiquinone and catecholate ligands. These complexes represent an interesting reversal on mixed-valence metal complexes. Just as electron transfer between metal centers exists as a property of these complexes, intramolecular interligand electron-transfer reactions are possible for the mixed-charge ligand molecules. While reactions of this type have not been studied in detail for transition-metal complexes, Prokof'ev and Kabachnik have reported studies on interligand electron transfer for mixed-charge quinone complexes of main group elements.[29]

Studies of magnetic coupling between a paramagnetic metal and an organic radical are not common. The semiquinone complexes provide an opportunity to study antiferromagnetic metal–radical coupling in well-characterized complexes, and the $M_4(DBSQ)_8$, M = Mn, Co, Ni, complexes have been of particular interest. Modeling studies on the Co and Ni complexes showed that a reasonable fit to the temperature-dependent paramagnetism could be obtained by considering only the metal–semiquinone coupling in the $M(DBSQ)_2$ units of the tetranuclear molecule.[10] The isostructural manganese complex $Mn_4(DBSQ)_8$ has a room-temperature magnetic moment of 10.2 μ_B (286 K) per Mn_4 molecule, a value also showing evidence of metal–semiquinone antiferromagnetic coupling. However, as the temperature of this complex is decreased to 10 K, the magnetic moment increases to 11.3 μ_B. This ferromagnetic behavior is the result of coupling between metals through the semiquinone oxygen bridges. Not all of the Mn–Mn interactions are necessarily ferromagnetic, but the strongest give rise to the net ferromagnetism of the complex. Both $Fe_4(DBSQ)_4(DBCat)_4$ and $Mn_4(DBSQ)_8$ contain d^5 metal ions but differ in that two of the bridging ligands that are semiquinone in the Mn_4 complex are reduced catecholates in the Fe_4 molecule. The bridging atoms associated with these ligands are O3 and the triply bridging oxygen O5. This difference in ligand charge, with the concomitant change in the orbital structure of the bridge, could lead to a change in the nature of the coupling interaction between metal ions. It is of interest that this change in net magnetic exchange interaction occurs without a structural change beyond that expected from the difference in radii of the metal ions.

Finally, it is of interest to consider the structural similarity between $Fe_4(DBSQ)_4(DBCat)_4$ and the $Fe_4(\mu\text{-}OH)_2$ core, which appears in various mineral structures. The centrosymmetric inner structure of polymeric leucophosphite, $K_2[Fe_4(OH)_2(PO_4)_4(H_2O)_2]\cdot 2H_2O$ and the mixed-valence iron mineral melonjosephite, $Ca_2[Fe_4(OH)_2(PO_4)_4]$ is shown (I).[27] Hydroxo oxygen atoms,

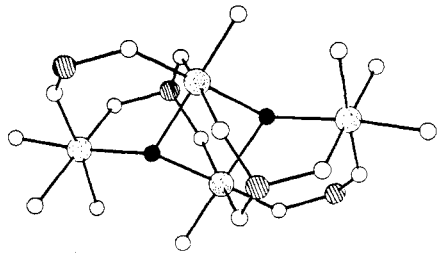

(I)

colored black in the drawing, are located atop triangular faces of the planar Fe_4 metal core in the same way that catecholate oxygens O5 and O5′ occupy triply bridging positions in the present structure. In both structures the Fe–Fe edge common to both triangular units has the shortest length, 3.108 Å for the leucophosphite structure, with longer lengths for the outer edges of the Fe_3 triangles. Edge bridging catecholate and semiquinone oxygens contribute to shorter Fe–Fe lengths in $Fe_4(DBSQ)_4(DBCat)_4$ and to stronger magnetic coupling between metal ions. Outer edge lengths in leucophosphite are 3.778 and 3.820 Å, and the room-temperature magnetic moment of 5.13 μ_B per iron shows evidence of weak antiferromagnetic coupling.[30]

General structural features of the inner core of $Fe_4(DBSQ)_4(DBCat)_4$ and the related tetranuclear semiquinone complexes appear common to a wide variety of materials ranging from natural and synthetic basic Fe_4O_2 and $Fe_4(OH)_2$ complexes to the tetranuclear alkoxides typified by $[Ti(OEt)_4]_4$.

Acknowledgment. This research was supported by the National Science Foundation under Grants CHE 85-03222 and CHE 88-

(28) Buchanan, R. M.; Pierpont, C. G. *J. Am. Chem. Soc.* **1980**, *102*, 4951.

(29) (a) Prokof'ev, A. I.; Kasymbekova, Z. K.; Bubnov, N. N.; Solodovnikov, S. P.; Khodak, A. A.; Kabachnik, M. I. *Isv. Akad. Nauk. SSSR* **1987**, 65. (b) Prokof'ev, A. I.; Khodak, A. A.; Malysheva, N. A.; Petrovskii, P. V.; Bubnov, N. N.; Solodovnikov, S. P.; Kabachnik, M. I. *Dokl. Akad. Nauk. SSSR* **1978**, *240*, 92. (c) Prokof'ev, A. I.; Prokof'eva, T. I.; Bubnov, N. N.; Solodovnikov, S. P.; Belostotskaya, I. S.; Ershov, V. V.; Kabachnik, M. I. *Dokl. Akad. Nauk. SSSR* **1977**, *234*, 603, 845.

(30) Rossman, G. R. *Am. Mineral.* **1976**, *61*, 933.

09923 (C.G.P.) and by the National Institutes of Health under Grant HL-13652 (D.N.H.).

Registry No. DBBQ, 3383-21-9; $Fe(DBSQ)_3$, 64020-89-9; $Fe_4(DBSQ)_4(DBCat)_4^-$, 119009-91-5; $Fe(CO)_5$, 13463-40-6.

Supplementary Material Available: Complete listings of anisotropic thermal parameters and hydrogen atom coordinates $Fe(DBSQ)_3$ and $Fe_4(DBSQ)_4(DBCat)_4$ (7 pages); observed and calculated structure factors (63 pages). Ordering information is given on any current masthead page.

Communications to the Editor

Dehydroquinate Synthase: A Sheep in Wolf's Clothing?

Theodore Widlanski, Steven L. Bender,[1] and Jeremy R. Knowles*

Department of Chemistry, Harvard University Cambridge, Massachusetts 02138

Received October 17, 1988

The shikimate pathway[2,3] is responsible for the biosynthesis of aromatic amino acids in plants and microorganisms. The second enzyme of this metabolic sequence, dehydroquinate synthase, catalyzes the conversion of the seven carbon keto acid 3-deoxy-D-*arabino*-heptulosonate 7-phosphate (DAHP, **1**) to dehydroquinate (DHQ, **2**), which is the first carbocyclic metabolite in the pathway. As is shown in Scheme I, the enzyme, which is a monomer of M_r 38 880, appears to catalyze an unusually complex concatenation of chemical changes.[4] The secondary alcohol at C-5 of DAHP is oxidized by enzyme-bound NAD^+, facilitating the β-elimination of inorganic phosphate across C-6 and C-7. After reduction of the C-5 ketone, the pyranose ring opens, and a subsequent intramolecular aldol reaction yields the product dehydroquinate. Following the recent suggestion that DHQ synthase may not, in fact, mediate the last two steps of Scheme I,[5] we now report experiments that suggest that the enzyme plays only a minor role in the second step of the sequence.

Recent work in our laboratory has shown that the enzyme-catalyzed elimination of inorganic phosphate occurs with syn stereochemistry from the cyclic α-pyranose form of the substrate.[6] This result is in accord with the stereochemical course of all enzymes that catalyze β-eliminations from ketones or from thioesters[7] and suggests that the elimination of P_i from DAHP is a stepwise (E1cB) process. If this is true, the *minimum* number of enzyme-bound species associated with the overall reaction is seven! While examining the behavior of substrate analogues that cannot complete the sequence shown in Scheme I, we have studied several carbocyclic DAHP analogues (e.g., **3**, **4**, **5**, and **6**)[8] that can be oxidized at C-5 and suffer abstraction of the C-6 proton, but that cannot complete the elimination reaction because the phosphate group has been converted into a phosphonate.

The homophosphonate analogue **3**, which is isosteric with DAHP, has a K_i value (1.7 μM) that is close to the K_m of DAHP

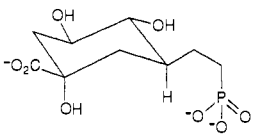

3

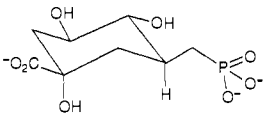

4

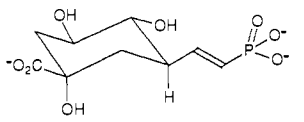

5

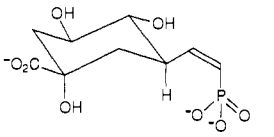

6

($\sim$4 μM).[9] Incubation of **3** with the enzyme in D_2O leads to enzyme-catalyzed exchange of the C-6 proton with the solvent.[11] In contrast, the phosphonate analogue **4** binds much more tightly to DHQ synthase[10] (this analogue is the best inhibitor of the enzyme yet found: $K_i \sim 0.8$ nM), and despite the fact that **4** is readily oxidized at C-5 when bound,[12] *no* exchange of the C-6 proton with the solvent is observed. The positioning of the phosphonate group is evidently critical (albeit in different ways) both for binding and for proton exchange.

To define the position of the phosphate ester group of enzyme-bound DAHP, we have examined the behavior of the unsaturated analogues **5** and **6**. The *E*-vinyl homophosphonate **5** mimics an expected low-energy conformation of the substrate DAHP and of the homophosphonate **3**, with the side chain in an enforced extended conformation. The *E*-vinyl analogue **5** is weakly bound by DHQ synthase ($K_i \sim 25$ μM), no oxidation at C-5 can be observed even at saturating concentrations, and no proton exchange at C-6 is detectable. In contrast, the *Z*-vinyl homophosphonate **6** inhibits the enzyme even better than the saturated analogue **3** ($K_i \sim 0.16$ μM), is oxidized to the same extent, and undergoes C-6 proton exchange at the same rate as does **3**. The *Z*-vinyl homophosphonate **6** is thus the only analogue that is *both* tightly bound *and* exchanges its C-6 proton with the solvent.[13]

(1) National Institutes of Health Post-Doctoral Fellow. Present address: Department of Chemistry, University of California–Irvine, Irvine, CA 92717.

(2) (a) Haslam, E. *The Shikimate Pathway*; Wiley: New York, 1974. (b) Weiss, U.; Edwards, J. M. *The Biosynthesis of Aromatic Compounds*; Wiley: New York, 1980.

(3) Kishore, G. M.; Shah, D. M. *Annu. Rev. Biochem.* **1988**, *57*, 627.

(4) (a) Srinivasan, P. R.; Rothschild, J.; Sprinson, D. B. *J. Biol. Chem.* **1963**, *238*, 3196. (b) Rotenberg, S. L.; Sprinson, D. B. *J. Biol. Chem.* **1978**, *253*, 2210.

(5) Bartlett, P. A.; Satake, K. *J. Am. Chem. Soc.* **1988**, *110*, 1628.

(6) Widlanski, T. S.; Bender, S. L.; Knowles, J. R. *J. Am. Chem. Soc.* **1987**, *109*, 1873.

(7) Schwab, J. M.; Klassen, J. B.; Habib, A. *J. Chem. Soc., Chem. Commun.* **1986**, 357.

(8) The carbocyclic analogue series was originally designed to complement the 2-deoxy substrate analogues,[6] neither of which can suffer ring opening after the elimination of P_i. Satisfactory spectroscopic data were obtained for all new compounds. Details of the synthetic work will be published elsewhere.

(9) At pH 7.5, 20 °C, in 50 mM potassium 3-(*N*-morpholino)propanesulfonate buffer containing $CoSO_4$ (50 μM), NAD^+ (10 μM), and substrate, using the *E. Coli* enzyme (Frost, J. W.; Bender, J. L.; Kadonaga, J. T.; Knowles, J. R. *Biochemistry* **1984**, *23*, 4470) coupled to dehydroquinase (1 unit) and monitored at 234 nm. Earlier reports (e.g. ref 10) of higher K_m values appear to derive from the use of a less sensitive assay method and the difficulty of obtaining true initial rates at the low substrate concentrations required.

(10) This behavior parallels that shown earlier for the pyranose derivatives: Le Marĕchal, P.; Froussios, C.; Level, M.; Azerad, R. *Biochem. Biophys. Res. Commun.* **1980**, *92*, 1104.

(11) The rate of proton exchange is approximately 0.1% of k_{cat}.

(12) The formation of enzyme-bound NADH is observed at 340 nm. The proportion of the enzyme that contains NADH and oxidized substrate analogue seems to be related to the redox potential of the analogue and approaches 100% for **3**, 4, and **6**.

(13) Although molecular mechanics calculations show that the charged groups of 4 and **6** are positioned similarly, the attack trajectory required for an intramolecular deprotonation in 4 and that required for intramolecular deprotonation in **6** are substantially different. The barrier for proton transfer via a five-membered ring may be more than 3 kcal/mol higher than that for a six-membered ring (Menger, F. M. *Tetrahedron* **1983**, *39*, 1025).

0002-7863/89/1511-2299$01.50/0